Available online at www.sciencedirect.com
ScienceDirect
Scripta Materialia 63 (2010) 480–483
Scripta MATERIALIA
www.elsevier.com/locate/scriptamat

Mechanical properties of Cu_6Sn_5 intermetallic by micropillar compression testing

L. Jiang and N. Chawla*

Materials Science and Engineering, Arizona State University, Tempe, AZ 85287-6106, USA

Received 19 March 2010; revised 18 April 2010; accepted 7 May 2010
Available online 12 May 2010

The micromechanical behavior of single-crystal Cu_6Sn_5 was studied by microcompression testing of pillars. The pillars were fabricated by focused ion beam milling and tested using a nanoindenter with a flat tip. The stress–strain behavior and fractographic analysis show that Cu_6Sn_5 deforms elastically and undergoes cleavage, resulting in fracture. The strain bursts on stress–strain curves correspond to cleavage on various planes. The fracture stress calculated using the area at the top of pillars was independent of taper angle.

Keywords: Lead-free solder; Focused ion beam; Micropillar compression; Cu_6Sn_5

With the increasing focus on developing environmentally benign electronic packages, Pb-free alloys have received a great deal of attention [1]. Most Pb-free solders are Sn-rich, with slight alloying additions of Ag and/or Cu. A Cu_6Sn_5 intermetallic layer grows from the reaction between the Sn-rich liquid and Cu substrate. The thickness and morphology of this Cu_6Sn_5 intermetallic layer significantly affect the mechanical performance of the solder [2,3]. For example, a relatively thin intermetallic layer may be beneficial in achieving a strong mechanical and chemical bond between Sn and Cu substrate [2,4]. At larger thickness, however, the intermetallic often acts as a crack initiation site, leading to catastrophic failure and poor toughness of the joint [3,5,6]. Thus, a fundamental understanding of the mechanical properties of Cu_6Sn_5 intermetallic is extremely important.

Characterizing the elastic and plastic properties of the Cu–Sn intermetallics is not trivial. Bulk intermetallics have been fabricated by casting and annealing processes [7–9], but these contain residual porosity and/or oxides. Furthermore, the intermetallic in the joint and that in bulk may differ significantly in grain size, defects, and crystallographic orientation. Indeed, preliminary studies on Young's modulus of Cu–Sn intermetallics show a large degree of variability [7–11]. Clearly, the properties of the actual intermetallics in the joint must be evaluated. This is quite a challenge, since the intermetallic reaction layers are of the order of only a few micrometers.

Instrumented indentation has been used to obtain the Young's modulus and hardness of Cu_6Sn_5 [12–16]. The fracture strength and strain-to-failure of this important intermetallic, however, has not yet been reported. In addition to a fundamental understanding of deformation of these materials, such information would be highly useful for more robust and accurate reliability-based models. In this study, we have used micropillar compression as a novel and unique means of probing the mechanical properties of Cu_6Sn_5. Micropillars were milled using focused ion beam (FIB) within single-crystal nodules of Cu_6Sn_5, and tested in compression using a nanoindenter with a flat tip.

Sn-rich alloy/Cu sandwich joints were prepared. High-purity Sn–3.9Ag–0.7Cu ingots (Indium, Ithaca, NY) were cut into squares approximately 6.35 mm × 6.35 mm × 1 mm. Oxygen-free copper bars (50.8 mm and 6.35 mm in thickness) were polished to a 0.05 μm finish with colloidal silica. A graphite mask was applied to the copper bars, leaving a 6.35 mm × 6.35 mm area for reflow. A rosin mildly activated (RMA) flux was applied to improve wetting between the copper and the solder. The joint was fixed within a copper fixture and the entire assembly was heated on a hot plate. The joints were heated to 120 °C for 2 min to allow the flux to burnout, followed by melting at 220 °C for 40 s. The assembly was then removed from the hot plate and air cooled on an aluminum heat sink. After cooling to room temperature, the joint was aged at 300 °C for 1 week to obtain a layer of Cu_6Sn_5 approximately 100–150 μm thick. The cross-section of the aged solder joint was polished to a final finish of 0.05 μm colloidal silica. Figure 1a shows

* Corresponding author. E-mail: nchawla@asu.edu

1359-6462/$ - see front matter © 2010 Acta Materialia Inc. Published by Elsevier Ltd. All rights reserved.
doi:10.1016/j.scriptamat.2010.05.009

the presence of two intermetallic layers of Cu_6Sn_5 and Cu_3Sn. Figure 1b shows the nodular Cu_6Sn_5 grains. Our previous work has shown that each of these nodules is a single crystal [17].

A dual-beam focused ion beam (FIB) with scanning electron microscope (SEM) (Nova 200 NanoLab FEG-SEM/FIB, FEI Co, Oregon) was used to mill micropillars of Cu_6Sn_5 in the single-crystal Cu_6Sn_5 nodules. Initially, a beam of Ga^+ ions at a current of 5 nA was used to mill out a circular trench with a diameter of about 25 μm and a coarse pillar in the center with a diameter of 5 μm. Then, a finer current of 30 pA was used to mill the pillar down to an average diameter of 2–3 μm. The aspect ratio (length/diameter) of the pillars was typically between 2 and 2.5. Several pillars in multiple grains were fabricated using this approach. Figure 1c shows an example of Cu_6Sn_5 pillars fabricated by FIB. The effect of taper angle of the pillar was also studied. By the standard milling approach, pillars with a taper angle of 4–8° were obtained. In order to minimize the taper of the pillar, the "ion-lathe" technique was used [18]. Here the sample is tilted so that the beam intersects the pillar tangential to the surface. By repeating this process over multiple small angle increments of 10°, a pillar with taper angles of 1–1.5° was obtained, as shown in Figure 1d.

The pillars were tested in compression using a nanoindenter (MTS XP, Agilent Technologies, Chandler, AZ). A Berkovich indenter (three-sided pyramid, Micromaterials, Wrexham, UK) with a flat triangular cross-section (10 μm on a side) was used. Experiments were performed at a nominal strain rate of 0.05 s^{-1}. A continuous measurement system (CSM) was used to measure the contact stiffness instantaneously as a function of indentation depth.

In order to obtain an accurate measurement of the actual displacement of the pillar, the elastic deformation of both the diamond indenter and the bulk substrate below the pillar were subtracted. This was done by using the equation by Sneddon [19,20], who considered the punching effect of a cylindrical punch indenting into an elastic half space. The displacement of the pillar is then given by:

$$d_p = d_{meas} - \frac{(1-\nu_i^2)}{E_i}\left(\frac{F_{meas}}{d_t}\right) - \frac{(1-\nu_b^2)}{E_b}\left(\frac{F_{meas}}{d_b}\right) \quad (1)$$

where d_p and d_{meas} represent the displacement of the pillar and the measured displacement by the instrument, respectively. F is the force, E_i and υ_i are the Young's modulus and Poisson's ratio of diamond (1141 GPa and 0.07 [21], respectively). E_b is the bulk Young's modulus of the base of the pillar, which in this case is also Cu_6Sn_5. υ_b is the Poisson's ratio of Cu_6Sn_5, which is taken to be 0.31 [14]. In order to obtain E_b, nanoindentation with a sharp tip was carried out in the individual grains. Young's modulus values for a given indentation were taken as the average value over a specimen depth where modulus was independent of depth, i.e. approximately 200–950 nm into the specimen. This yielded an average Young's modulus of 115.5 ± 4.1 GPa, which was independent of grain orientation.

Figure 2a shows the stress–strain curves of Cu_6Sn_5 obtained from microcompression testing. The stress–strain curve is linear until fracture of the pillars takes place. There are some strain bursts present on the stress–strain curves. Fractographic analysis was conducted to understand the nature of these strain bursts. The fractured pillars were imaged along the compression axis, shown in Figure 2b, as well from the side of the pillar, shown in Figure 2c. Multiple strain bursts are frequently observed in the compression testing of pure metal pillars, such as Ni [19,20,22]. Intermetallics, particularly at ambient temperature, have limited slip

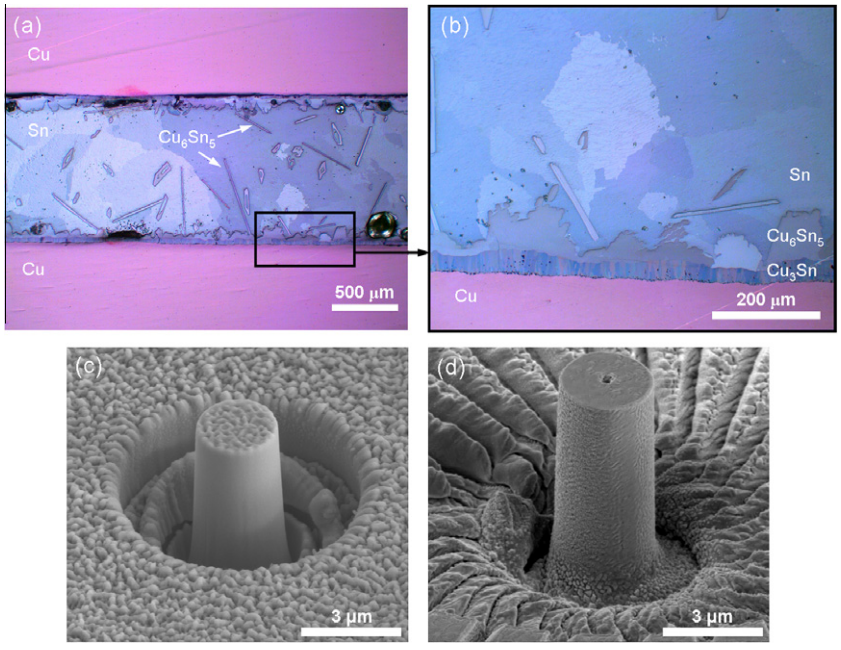

Figure 1. (a) A low-magnification optical micrograph of an as-aged solder joint showing the presence of two intermetallic layers of Cu_6Sn_5 and Cu_3Sn; (b) a high-magnification image showing nodule single-crystal Cu_6Sn_5 grains; (c) a pillar with a taper angle of ~4° fabricated using FIB; and (d) a taper-free pillar fabricated using the ion-lathe technique.

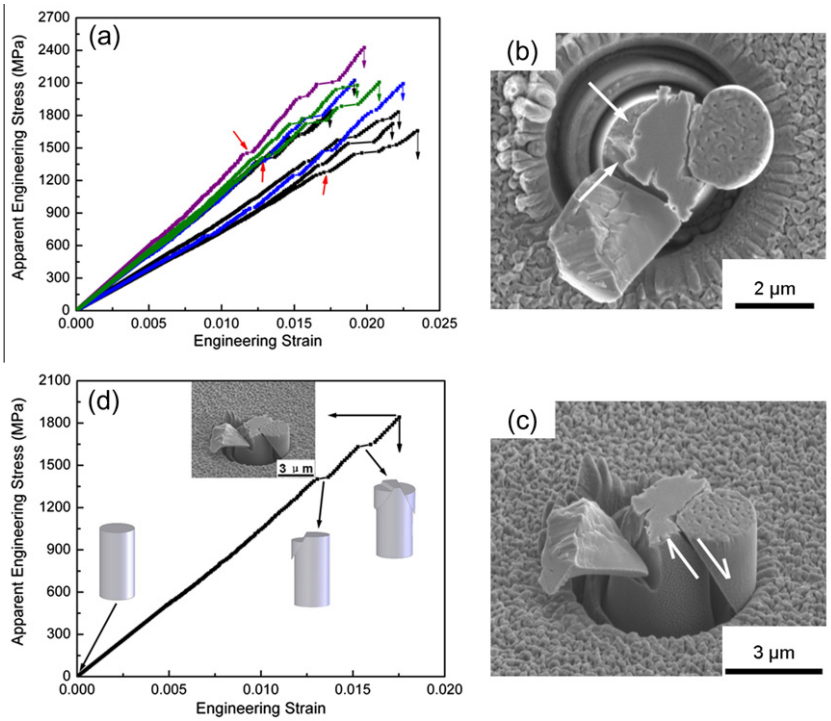

Figure 2. (a) The stress–strain curves of pillars in multiple single-crystal Cu_6Sn_5 grains with the presence of strain bursts, some of which are marked by red arrows. Curves of the same color are from a given grain. (b and c) Fractographic images of the compressed pillar observed using SEM (b, top view and c, side view). Cleavage on certain planes, i.e. marked by arrows in figure (b), is corresponds to strain bursts on the stress–strain curves. (d) A schematic showing the fracture of pillars during compression testing. (For interpretation of the references to color in this figure legend, the reader is referred to the web version of this paper.)

systems and high critical resolved shear stresses for slip. Furthermore, they deform by the motion of superpartial dislocations. Thus, the chances of multiple slip and dislocation avalanches in Cu_6Sn_5, as observed in pure metals such as Ni, are very small. It appears that the Cu_6Sn_5 pillars fracture by cleavage along certain crystallographic planes, resulting in fracture of the pillar. The strain bursts shown in Figure 2a are a result of the shearing along individual cleavage planes. The number of strain bursts varies between two and three, and these correspond to the number of cleavage planes observed in fracture surfaces (Fig. 2b). The evolution of fracture of pillars is shown schematically in Figure 2d. The first onset of cleavage occurs at a critical load. Then, cleavage takes place on another plane, followed by smashing of the top of the pillar. Thus, in these materials, the initial cleavage event corresponds to the fracture stress of the pillar, and the fracture stress of the pillars should be defined by the onset of the first strain burst. Based on this, the corrected stress–strain curves are shown in Figure 3a. It should be noted that studies of macroscopic fracture in the Sn–Cu_6Sn_5–Cu system have also reported that Cu_6Sn_5 fails by cleavage [23].

Several parameters, such as pillar taper, aspect ratio and crystallographic orientation, may affect micropillar compression behavior. All of the pillars tested had a similar aspect ratio (2–2.5). Zhang et al. [24] conducted numerical simulations that showed that the aspect ratio of pillars has a relatively small effect on the stress–strain behavior, especially for pillar aspect ratios larger than 2. It was also of interest to determine whether crystallography plays a role in mechanical stress of the nodules. There is some controversy about the crystal structure of Cu_6Sn_5 [25,26]. Our work seems to support that of Frear [25], who showed that the structure appears to be a superlattice based on a hexagonal unit cell. Using

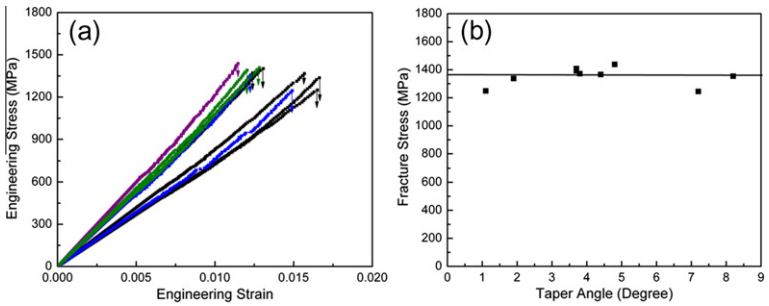

Figure 3. (a) The stress–strain curves of pillars until the onset of first strain bursts and (b) a plot showing the relation between top fracture stress and taper angle of pillars.

electron back-scattered diffraction (EBSD), we determined that Cu_6Sn_5 nodules grew along the *c*-axis of the unit cell and that the planes being compressed had a rotational symmetry along the *c*-axis of the unit cell [17]. Thus, it is not surprising that the pillars tested were somewhat independent of the nodule orientation.

The effect of taper angle on fracture stress was also examined and is shown in Figure 2c. The fracture stress is essentially independent of taper angle, if the nominal area at the top of the pillar is used, and is around 1356 ± 64 MPa. The strain to failure is around $1.37 \pm 0.18\%$. If one takes the average diameter of the pillar (using an average of the top and bottom diameters), then, of course, a linear decrease in strength with taper angle is observed. Zhang et al. [24] simulated the effect of taper on the mechanical behavior of pillars and reported that using an average area to calculate the stress will result in a significant underestimation of the stress when the pillar is tapered with an angle as low as 3°, which is consistent with what we have observed in this study.

In summary, we have tested multiple single-crystal nodules of Cu_6Sn_5 in compression using micropillars fabricated by FIB. The pillars were tested in both taper-free condition and with a taper angle of 4–8°. We have shown that Cu_6Sn_5 intermetallics are fairly brittle and that pillars fail by cleavage. The average fracture stress of the pillars was around 1356 MPa and the strain to failure was around 1.37%. The strain bursts on the stress–strain curves correspond to cleavage planes in the pillars. This is the first report describing the fracture stress and fracture mechanisms of the important intermetallic Cu_6Sn_5.

The authors are grateful for financial support from the Center for Engineering Materials (CEMAT) at Arizona State University. The authors thank Dr. Danny Singh for assistance with the FIB and Drs. Darrel Frear and Jason Williams for interesting discussions.

[1] N. Chawla, Int. Mater. Rev. 54 (2009) 368–384.
[2] P. Protsenko, A. Terlain, V. Traskine, N. Eustathopoulos, Scripta Mater. 45 (2001) 1439.
[3] D.R. Frear, JOM 48 (1996) 49.
[4] Y.C. Chan, A.C.K. So, J.K.L. Lai, Mater. Sci. Eng. B 55 (1998) 5.
[5] D.R. Frear, P.T. Vianco, Metall. Trans. A 25 (1994) 1509.
[6] R.E. Pratt, E.I. Stromswold, D.J. Quesnel, J. Electron. Mater. 23 (4) (1994) 375.
[7] R.J. Fields, S.R. Low III, G.K. Lucey Jr., in: M.J. Cieslak, J.H. Perepezko, S. Kang, M.E. Glicksman (Eds.), The Metal Science of Joining, TMS, Warrendale, PA, 1992, p. 165.
[8] B. Subrahmanyan, Trans. Jpn. Inst. Metals 130 (1972) 93.
[9] D.R. Frear, in: D.R. Frear et al. (Eds.), Mechanics of Solder Alloy Interconnects, Van Nostrand Reinhold, New York, 1994, p. 60.
[10] L.M. Ostrovskaya, V.N. Rodin, A.I. Kuznetsov, Soviet. J. Non-ferrous. Metall. (Tsvetnye Metally) 26 (1985) 90.
[11] H. Rhee, J.P. Lucas, K.N. Subramanian, J. Mater. Sci. 13 (2002) 477.
[12] X. Deng, N. Chawla, K.K. Chawla, M. Koopman, Acta Mater. 52 (2004) 4291–4303.
[13] R.R. Chromik, R.P. Vinci, S.L. Allen, M.R. Notis, J. Mater. Res. 18 (2003) 2251–2261.
[14] G. Ghosh, J. Mater. Res. 19 (2004) 1439–1454.
[15] G.Y. Jang, J.W. Lee, J.G. Duh, J. Electron. Mater. 33 (2004) 1103–1110.
[16] P.F. Yang, Y.S. Lai, S.R. Jian, J. Chen, R.S. Chen, Mater. Sci. Eng. A 485 (2008) 305–310.
[17] L. Jiang, N. Chawla, 2009, unpublished work.
[18] M.D. Uchic, D.M. Dimiduk, Mater. Sci. Eng. A 400–401 (2005) 268–278.
[19] C.A. Volkert, E.T. Lilleodden, Philos. Mag. 86 (2006) 5567–5579.
[20] C.P. Frick, B.G. Clark, S. Orso, A.S. Schneider, E. Arzt, Mater. Sci. Eng. A 489 (2008) 319–329.
[21] G. Simmons, H. Wang, Single Crystal Elastic Constants and Calculated Aggregate Properties: A Handbook, MIT Press, Cambridge, MA, 1971.
[22] D.M. Dimiduk, M.D. Uchic, T.A. Parthasarathy, Acta Mater. 53 (2005) 4065–4077.
[23] H.-T. Lee, M.-H. Chen, H.-M. Jao, T.-L. Liao, Mater. Eng. A358 (2003) 134–141.
[24] H. Zhang, B.E. Schuster, Q. Wei, K.T. Ramesh, Scripta Mater. 54 (2006) 181–186.
[25] D.R. Frear, Ph.D. thesis, University of California Berkeley, 1987, pp. 80–111.
[26] A.-K. Larsson, L. Stenberg, S. Lidin, Acta Crystallogr. B 50 (1994) 636–643.